



Ethanol Conversion to Short-Chain Olefins Over ZSM-5 Zeolite Catalysts Enhanced with P, Fe, and Ni

Ricardo H. Gil-Horán¹ · Juan C. Chavarría-Hernández¹ · Patricia Quintana-Owen² · Aída Gutiérrez-Alejandre³

Published online: 12 February 2020
© Springer Science+Business Media, LLC, part of Springer Nature 2020

Abstract

The ethanol dehydration and subsequent ethylene oligomerization to short-chain olefins using catalysts based on ZSM-5 zeolite was studied in detail. P, Fe, and Ni were added by incipient wetness impregnation on zeolites with two SiO₂/Al₂O₃ molar ratios (50 and 80). The catalysts were characterized by N₂ adsorption–desorption, XRD, SEM–EDX, FTIR spectroscopy of adsorbed pyridine, and XPS techniques, while the catalytic activity was evaluated using an isothermal fixed-bed reactor. The impregnation of P, Fe, and Ni significantly improved the formation of the desired C₃₊ olefins (olefins having three or more C atoms). Particularly, the zeolite with SiO₂/Al₂O₃ molar ratio = 50 and impregnated with P, exhibited the highest selectivity (C₃₊ olefins > 45 wt% at TOS = 5 h) in comparison with the rest of the evaluated catalysts. On the contrary, catalysts with SiO₂/Al₂O₃ molar ratio = 80 showed lower selectivity to C₃₊ olefins, producing more side products (i.e. paraffins, aromatics and diethyl-ether).

Keywords Ethanol to hydrocarbons · ZSM-5 zeolite · Short-chain olefins · Phosphorus · Iron · Nickel

1 Introduction

Light olefins, such as ethylene, propylene, and butylene, as well as other hydrocarbons, are useful not only as fuels but are considered important raw materials in the petrochemical industry [1]. Particularly, olefins of three or more carbon atoms (C₃₊ olefins) can be directly oligomerized to larger molecules in fewer reaction steps than ethylene, which makes them more desirable for some processes (e.g. synthetic fuel production). However, until now, they are

mainly produced from the cracking of fossil naphtha [2], and therefore, from production processes to final consumption, they favor the emission of greenhouse gases among other environmental problems [3]. In addition, the continued decline in oil-reserves and the high fluctuation of oil-prices have promoted in recent years a special interest in obtaining alternative fuels and high-value chemical compounds by implementing the use of biorefineries and using raw materials from renewable sources. Particularly, ethanol (EtOH) can be produced by the fermentation of biomass [4] and subsequently be catalytically transformed into higher value molecules (e.g. olefins), so it promises to be an alternative source to fossil hydrocarbons [5]. According to the “Renewable Fuels Association” [6], in 2018 the world production of ethanol reached 28.57 billion gallons, with the United States of America being the main producer followed by Brazil.

Ethanol can be transformed into ethylene and other short chain hydrocarbons (i.e. C₃₊ olefins, paraffins, aromatics and naphthenes) using ZSM-5 zeolite (Zeolite Socony Mobil-5), which is a crystalline and microporous catalyst [7], whose acidic and structural properties promote simultaneous reactions of dehydration, oligomerization, isomerization, cyclization, aromatization, hydrogen transfer and cracking. It has been found that the hydroxyl groups located between aluminum and adjacent silicon atoms are strongly acidic Brønsted sites

Electronic supplementary material The online version of this article (<https://doi.org/10.1007/s11244-020-01229-8>) contains supplementary material, which is available to authorized users.

✉ Juan C. Chavarría-Hernández
jc.ch@cicy.mx

¹ Unidad de Energía Renovable, CICY, Parque Científico y Tecnológico de Yucatán, Carretera Sierra Papacal–Chuburná Puerto, Km 5, Sierra Papacal, Mérida, Yucatán 97302, Mexico

² Departamento de Física Aplicada, CINVESTAV-IPN, Unidad Mérida, A.P. 73, Cordemex, Mérida, Yucatán 97310, Mexico

³ UNICAT, Departamento de Ingeniería Química, Facultad de Química, UNAM, Cd. Universitaria, Ciudad de México 04510, Mexico

that carry out acid-catalyzed reactions [8]. In several studies, ZSM-5 zeolite has been compared with other solid catalysts that exhibit different acidity and porosity [9, 10], or with a similar density of Brønsted acid sites but different pore structure [11]. The results have demonstrated its excellent activity in the dehydration reaction of ethanol to ethylene, and particularly its ability to obtain a complex mixture of short-chain hydrocarbons useful for the chemical and refining industry.

Recent studies [1, 2, 12–25] have evaluated the catalytic conversion of ethanol to olefins (mainly ethylene and propylene) and other hydrocarbons, using modified ZSM-5 zeolites. Generally, catalyst post-treatments such as impregnation, ion exchange, alkali treatment or steaming, are carried out to increase the hydrothermal stability and enhance the catalytic activity [5]. The addition of different compounds of Ba, Ca, Fe, La, Mg, Mn, P, Sr, Zr, Ni, Mo, Zn, and Ga has been studied, both by ion exchange and by impregnation methods, seeking to enhance the reaction selectivity to the desired products. However, it has been found that in some cases, after post-treatment, the acidity decreases because of a partial dealumination [23].

Specifically, it has been reported the enhancement of the catalytic-performance of ZSM-5 zeolite by impregnating phosphorus (P), iron (Fe), or nickel (Ni) [1, 2, 13, 15, 17, 19, 26–28], thereby increasing the yield and selectivity to olefins, particularly ethylene and propylene. In addition, an improvement of the hydrothermal stability, in comparison with unmodified ZSM-5 zeolites or where other metals were used, has been observed. However, a comparison of the referred works is not an easy task, because of differences in synthesis procedures, catalyst composition and reaction conditions. Furthermore, the reported selectivity to C_{3+} olefins is low in most cases. Particularly, Phung et al. [27] evaluated the impregnation of P, Fe and Ni on ZSM-5 zeolite with SiO_2/Al_2O_3 molar ratio = 50 for this reaction, but the authors reported only the gas products, without including the produced liquid hydrocarbons. They claim that the addition of P promotes the appearance of weaker Brønsted acidic P–OH groups, while the impregnated Fe and Ni species carry Lewis acidity.

According to the above, the aim of the present work is to investigate the conversion of ethanol to C_{3+} olefins over eight ZSM-5 zeolite catalysts of two SiO_2/Al_2O_3 molar ratios and impregnated with P, Fe or Ni. Additionally, the effects of the impregnation on the catalyst properties, on the catalytic activity and the reaction selectivity, were studied in detail.

2 Experimental

2.1 Catalyst Preparation

Commercial zeolites were used as NH_4 -ZSM-5 ammoniacal state (Zeolyst, CBV5524G and CBV8014, with SiO_2/Al_2O_3 ratio = 50 and 80 mol mol⁻¹, respectively), which

were calcined at 550 °C with O_2 flow for 3 h with a heating ramp of 1 °C min⁻¹, obtaining the H-ZSM-5 acid form. Subsequently, catalysts loaded with 1 wt% of P, Fe, and Ni, were prepared by incipient wetness impregnation. To this end, solutions of $(NH_4)_2HPO_4$, $FeCl_3 \cdot 6H_2O$ and $Ni(NO_3)_2 \cdot 6H_2O$ (Sigma Aldrich) were added dropwise to H-ZSM-5 zeolite and allowed to dry for 24 h at room temperature. Then, it was dried at 120 °C for 5 h and immediately calcined at 550 °C with O_2 flow for 5 h with a heating ramp of 1 °C min⁻¹. In total, eight catalysts were obtained: two non-impregnated [H-ZSM-5-(X)] and six impregnated [M-ZSM-5-(X)], where M is P, Fe, or Ni, and X is the nominal value of the SiO_2/Al_2O_3 molar ratio.

2.2 Catalyst Characterization

The textural properties were measured by N_2 adsorption–desorption in a BELSORP-max equipment ($P/P_0 = 0.99$ and 77 K) using the BET method to calculate the surface area, t-plot and MP-plot to determine the diameter and the size distribution of micropores, respectively [29]. The solid samples were previously degassed with a vacuum of 0.2 Pa at 400 °C for 2 h.

The morphology of the catalysts and the elemental-composition were studied by scanning electron microscopy and energy-dispersive X-ray spectroscopy (SEM–EDX) using a JEOL-JSM-6360-LV high-resolution microscope coupled to an EDX detector, with acceleration voltages of 20 kV and 25 kV. Likewise, the oxidation state of the impregnated particles was determined by X-ray photoelectron spectroscopy (XPS) in a Thermo Scientific K-ALPHA Surface Analysis equipment, with a 180° double-focus hemispheric analyzer and a 128 channels detector at 2×10^{-9} mbar, using an aluminum monochrome Al-K α radiation source (1486.6 eV, 12 kV and 40 watts) with relative incidence angle of 30°. The XPS spectra were processed with the CasaXPS software (version 2.3.19) in which the baseline modeling was performed by Shirley background subtraction method, while peak deconvolutions were carried out using the GL(X) decomposition parameter [Gaussian(Y%)–Lorentzian(X%), where $Y = 100 - X$], being Gaussian(20%)–Lorentzian(80%) the combination that allowed the best fit for peak modeling.

The crystalline structure of the catalysts was analyzed at room temperature by X-ray diffraction (XRD) in a Bruker D2-Phaser equipment with a copper anode, Cu-K α radiation ($\lambda = 1.5406 \text{ \AA}$, 30 kV and 10 mA) over 2θ values in the range of 5°–50° at the scanning rate of 0.01° s⁻¹.

Fourier Transform Infrared (FTIR) spectra were recorded with a Thermo Scientific Nicolet 6700 FTIR spectrometer (4 cm⁻¹ of spectral resolution and 100 scans). The samples were pressed into thin wafers ($\approx 7.48 \text{ mg cm}^{-2}$) and outgassed at 450 °C for 2 h, then were

contacted with pyridine (Py) vapor (20 mmHg) as probe molecule at room temperature for 15 min. The pyridine was subsequently evacuated by thermal desorption under vacuum (9×10^{-5} Torr), first at room temperature, then at 150 °C, and finally at 300 °C, for 15 min each temperature. FTIR spectra were recorded before and after pyridine adsorption and after each evacuation step. Then, the difference spectra were obtained by subtracting the spectrum of the outgassed sample from the spectra recorded after the adsorption/desorption steps. The concentrations of both Brønsted and Lewis acid sites after desorption at 150 °C and 300 °C were calculated by the Eq. (1) [30, 31] using the integrated absorbance of the 1545 cm^{-1} band related to pyridinium ions (PyH^+) and the 1450 cm^{-1} band related to Lewis bonded pyridine (PyL), respectively. This was done by fitting the FTIR difference spectra with a Gaussian–Lorentzian function and baseline modelling using the ORIGIN software. Additionally, the distribution of the acid strength of the Brønsted sites was determined assuming that, after desorption at 150 °C, the concentration of the acid sites for the band at 1545 cm^{-1} corresponds to the total (strong and weak) Brønsted acid sites, while the remaining concentration after desorption at 300 °C, corresponds to the strong Brønsted acid sites. The same consideration was made to determine the distribution of the acid strength of the Lewis sites, using the concentrations calculated for the band at 1450 cm^{-1} after desorption at 150 °C and 300 °C.

$$n_T = \frac{A_L C_d}{\epsilon_L m} + \frac{A_B C_d}{\epsilon_B m} \quad (1)$$

In Eq. (1) n_T is the number of pyridine molecules ($\mu\text{mol g}^{-1}$) that remain adsorbed after evacuation at temperature T , which is equivalent to the total concentration of acid sites. A is the integrated absorbance (cm^{-1}) of FTIR bands related to pyridine adsorbed at Brønsted acid sites (B) or at Lewis acid sites (L). C_d and m are the cross-sectional area (cm^2) and mass (g) of the sample wafer, respectively. ϵ is the molar absorption coefficient ($\text{cm } \mu\text{mol}^{-1}$), also known as integrated molar extinction coefficient, of pyridine adsorbed at Brønsted acid sites (B) or at Lewis acid sites (L). The integrated molar extinction coefficient values reported by Emeis [32] were used: 1.67 $\text{cm } \mu\text{mol}^{-1}$ for the 1545 cm^{-1} band (Brønsted acid sites) and 2.22 $\text{cm } \mu\text{mol}^{-1}$ for the 1450 cm^{-1} band (Lewis acid sites); which have been widely cited and validated for Si/Al-based catalyst, including ZSM-5 zeolite [30, 31, 33].

2.3 Catalytic Activity Testing

Continuous reactions were carried out in a 316 stainless steel isothermal fixed-bed reactor, of 9 mm internal diameter and 5 cm long of the effective isothermal volume, mounted in a MICROACTIVITY-REFERENCE system, which has a Peltier cell for liquid condensation, and an automatic process-variable control system. The gas outlet of the condenser was on-line connected to a gas chromatograph YL-Instrument-6500GC coupled to a mass detector YL6900GC/MS. For the gas product analysis, an Agilent GS-Carbonplot capillary-type column of 30 m long, 0.320 mm internal diameter, and 1.5 μm of film thickness was used. Concerning the condensed products, two liquid phases were obtained, of which, the hydrocarbon phase (supernatant) was analyzed in the same way by GC-mass spectrometry using an EST-Analytical-FLEX automatic injector and a Mega-5 HT capillary-type column of 30 m long, 0.250 mm internal diameter, and 1.5 μm of film thickness.

Reactions were carried out using 0.5 g of powdered catalyst with particle size of 250 to 420 μm (60 to 40 mesh). Each catalyst was previously conditioned in situ for 1 h at 35 bar and 450 °C, with 60 mL min^{-1} of N_2 flow to remove moisture and adsorbed impurities. For each reaction, ethanol–water mixture at 95 vol% (0.1115 mL min^{-1}) using a GILSON-307 HPLC pump with an integrated flow control, and N_2 (102.5 mL min^{-1}) as carrier gas using a Bronkhorst EL-FLOW Select F-201CV flow controller, were fed to the reactor. The reactions were carried out for 5 h of time on stream (TOS = 5 h) at 35 bar, 350 °C, and WHSV = 10 [$\text{g}_{\text{EtOH}} \text{g}_{\text{cat}}^{-1} \text{h}^{-1}$]. The reaction conditions were selected based on preliminary at-home studies focused on the formation of C_{3+} olefins, and in particular, the operating pressure obeys an integrated process scheme under development, in which it is mainly sought to obtain hydrocarbons in the range of jet fuel. Every 60 min, the gas products were measured by GC-Mass spectrometry, and the condensed liquids were recovered in vials for further analysis. The mass balance of the reaction products was carried out by classifying the formed hydrocarbons into product families (olefins, paraffins, aromatics, naphthenes and diethyl-ether), and the performance of the catalysts was evaluated. The liquid hydrocarbon yield was calculated by Eq. (2), and the product mass selectivity was determined by Eq. (3). Particularly, the formation of C_{3+} olefins versus the generation of side products was studied.

$$\text{Liq. HC yield} = \frac{F_{\text{Liq}} - (\text{EtOH}^0)(0.39114) - W^0}{\text{EtOH}^0} \times 100 \quad (2)$$

$$\text{Selectivity } (S_i) = \frac{M_i}{\sum_{i \neq \text{EtOH}} M_i} \times 100 \quad (3)$$

The nomenclature in Eq. (2) and Eq. (3) is as follows: F_{Liq} is the mass flow of the liquid fraction (hydrocarbon + water) recovered at the output of the reactor, $EtOH^0$ and W^0 are the mass flows of pure ethanol and water fed to the reactor, respectively. S_i is the product mass selectivity (wt%), and M_i is the normalized mass fraction on a dry basis of i hydrocarbon product-family in the reactor effluent (liquids + gases).

3 Results and Discussions

3.1 Catalyst Characterization

The catalysts impregnated with P, Fe, and Ni showed a slight decrease in the BET surface area and the volume of the micropores compared to the non-impregnated H-ZSM-5 catalysts (Table 1). This effect has been attributed to the particle deposition on the surface of the catalysts, partially blocking the micropores [1, 13, 26, 34], whose diameters (D_{MICRO}) were found to be in the range of 0.40 to 1.60 nm with maximum distribution peaks between 0.6 and 0.7 nm (Fig. 1). This result is typical of ZSM-5 zeolite corresponding to the MFI structure [35, 36]. Likewise, all the materials showed type 1 adsorption isotherms with hysteresis cycle of type H_4 formed in the range of $0.47 < P/P_0 < 0.98$ (Fig. S1 in supplementary material), which corresponds to pores with channels without interconnection, or agglomerated particles that form pores with cavities.

The SEM micrographs (Fig. 2) show agglomerated crystals with the characteristic shape of ZSM-5 reported by other authors [14, 37]. No changes were observed in the

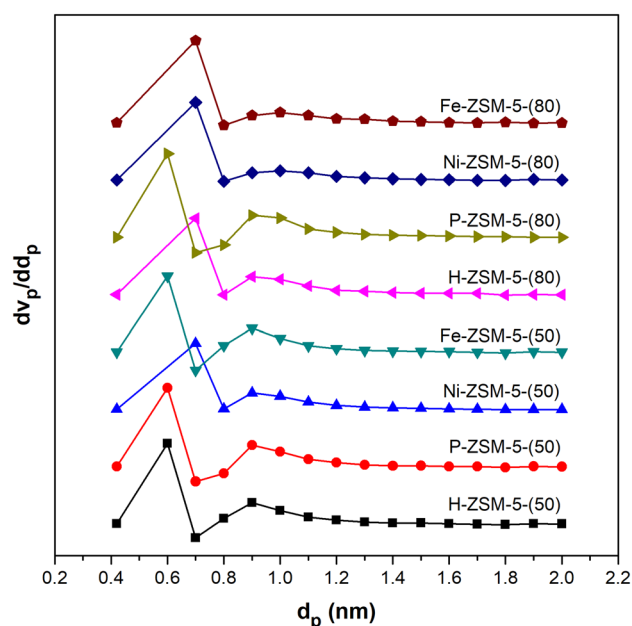


Fig. 1 Micropores diameter distribution by the MP-Plot method

structure and morphology of the zeolites after impregnation. However, it is noteworthy that agglomerates of ZSM-5 with SiO_2/Al_2O_3 ratio = 80 mol mol^{-1} are larger than those with a ratio of 50 mol mol^{-1} . On the other hand, the EDX analysis allowed to know the surface composition of the catalysts (Table 1). It stands out that the measured content of P, Fe, and Ni was less than 1 wt% on the surface, suggesting a possible incorporation of the particles at a less superficial level in the catalysts. Additionally, the SEM–EDX mapping shows that there was a good dispersion of P, Fe, and Ni particles on the surface of the zeolites (Fig. S2 in supplementary material). These results indicate that the particles of P, Fe, and Ni

Table 1 Textural properties and elemental composition of the catalysts

Catalyst	$SiO_2/Al_2O_3^a$ mol mol ⁻¹	S_{BET}^b (m ² g ⁻¹)	V_{MICRO}^c (cm ³ g ⁻¹)	O ^d (wt%)	Al ^d (wt%)	Si ^d (wt%)	M ^d (wt%)
H-ZSM-5-(50)	50	436.86	0.1794	64.46	1.04	34.50	–
Ni-ZSM-5-(50)	50	413.03	0.1748	60.83	1.12	37.25	0.80
Fe-ZSM-5-(50)	50	416.38	0.1760	63.17	1.02	35.04	0.77
P-ZSM-5-(50)	50	392.01	0.1587	63.00	1.13	35.04	0.83
H-ZSM-5-(80)	80	453.59	0.1949	59.01	0.86	40.13	–
Ni-ZSM-5-(80)	80	384.76	0.1586	60.85	0.80	37.49	0.87
Fe-ZSM-5-(80)	80	411.95	0.1720	60.22	0.80	38.02	0.96
P-ZSM-5-(80)	80	416.40	0.1841	60.89	0.90	37.37	0.84

^aNominal molar ratio reported by the manufacturer for the non-impregnated zeolites

^bBET specific surface area

^cMicropores volume by t-plot method

^dElemental composition by EDX (M = P, Fe or Ni)

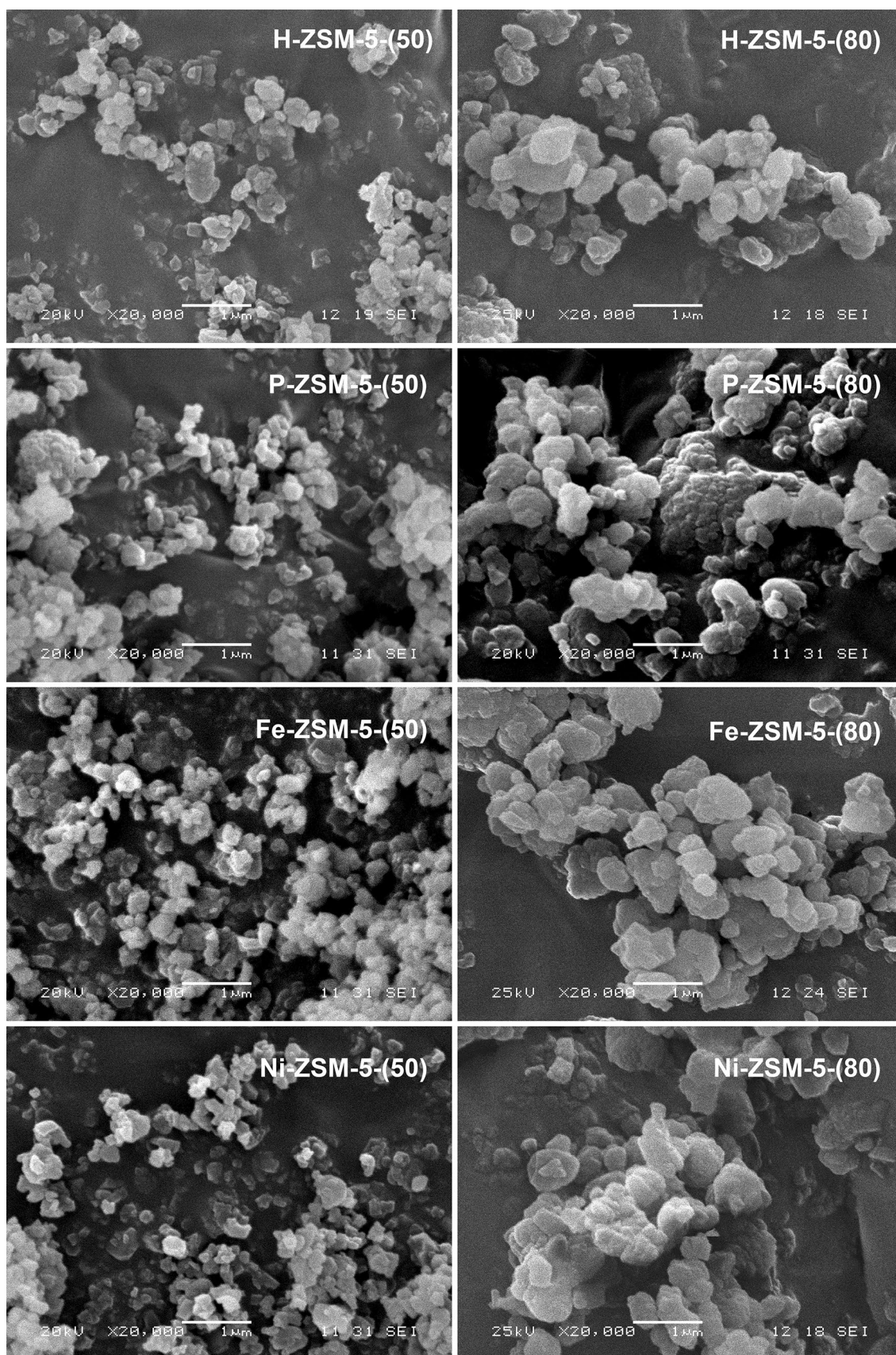


Fig. 2 SEM micrographs of impregnated and non-impregnated catalysts

were incorporated mainly on the surface and therefore did not cause a modification of the crystalline structure.

The X-ray diffraction patterns obtained at 2θ angle (Fig. 3) are characteristic of the MFI structure [38] and show that the impregnation did not cause significant changes on crystallinity, which agrees with those reported in previous studies [12, 17, 37]. No additional crystalline phases of P, Fe, and Ni (either elemental or oxide state) were detected by XRD because of their low concentration and dispersion.

The XPS analysis allowed to determine the oxidation states of P, Fe, and Ni particles impregnated on the surface of the catalysts, even though their low concentration.

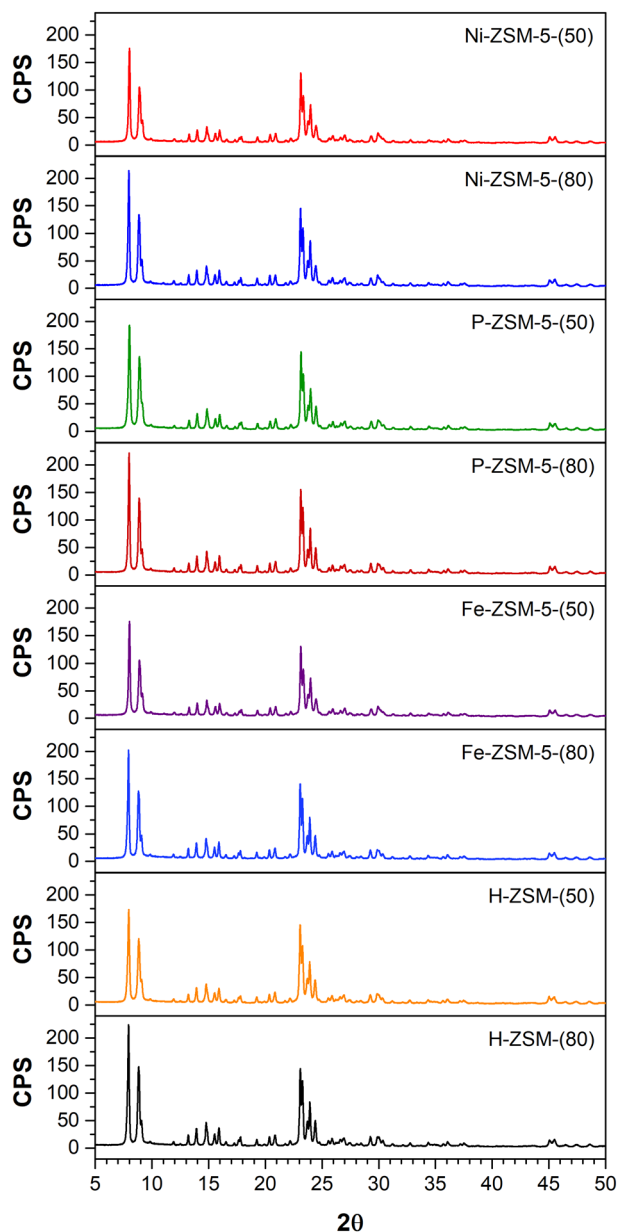


Fig. 3 XRD patterns of impregnated and non-impregnated catalysts

The spectra showed slight peaks whose binding energy directly depends on the valence number of the particles. The iron impregnated catalysts showed main peaks of Fe-2p_{3/2} and Fe-2p_{1/2} with approximate binding energies of ~711.15 eV and ~724 eV respectively, as well as satellite peaks around ~716.85 eV and ~732.5 eV (Fig. 4a), which correspond to the Fe₂O₃ spectrum [39–43] with Fe⁺³ oxidation state. For the nickel impregnated catalysts, main peaks of Ni-2p_{3/2} and Ni-2p_{1/2} were observed with approximate binding energies of ~854.5 eV and ~872 eV respectively, as well as satellite peaks around of ~859 eV and ~879.5 eV (Fig. 4b), which correspond to the NiO spectrum [39, 44] with Ni⁺² oxidation state. Finally, the phosphorus impregnated catalysts showed a peak P-2p with approximate binding energy of ~135 eV (Fig. 4c), which corresponds to the spectrum of P₂O₅ [45, 46] with P⁺⁵ oxidation state. Particularly, in the case of phosphorus, no evidence demonstrating its integration into the structure of ZSM-5 zeolite was found, as suggested by other authors with respect to the formation of an amorphous extra-framework aluminophosphate, P(OH)₄⁺, PO(OH)₂⁺ or H₃P₂O₇⁺ cations [47], or by the occupation of silicon sites to form (SiO)_xAl(OP)_{4-x} species (x = 1 to 4) [48].

Figure 5 shows the FTIR subtraction spectra in the range of 1700 cm⁻¹ to 1350 cm⁻¹ of the pyridine species that remain adsorbed after evacuation at 150 °C and at 300 °C. Two bands with vibrational mode ν 19b near 1397 cm⁻¹ and 1546 cm⁻¹ were identified, as well as a band with ν 8a vibrational mode around 1637 cm⁻¹, attributed to pyridinium ions (PyH⁺) adsorbed on Brønsted sites [33, 49]. Similarly, the IR bands on the 1450–1445 cm⁻¹ region with vibrational mode ν 19b, and the bands at 1612 cm⁻¹ and at 1622 cm⁻¹ (ν 8a), are identified as molecular pyridine covalently coordinated on Lewis acid sites (PyL) [33, 49, 50]. Additionally, the bands at 1598 cm⁻¹ (ν 8a) and at 1440 cm⁻¹ (ν 19b) are assigned to hydrogen bonded pyridine to hydroxyl groups (silanol groups) [50]. Particularly, the band at 1440 cm⁻¹ was observed as a shoulder attached to the 1446 cm⁻¹ band only in the non-impregnated and evacuated at 150 °C H-ZSM-5-(50) catalyst, which subsequently disappeared after evacuating at 300 °C. Finally, the band at 1491 cm⁻¹ (ν 19a) is related to adsorbed pyridine on both Brønsted and Lewis sites [33, 49].

Table 2 shows the strong and weak acid sites concentration and the acid strength distribution for the catalysts with SiO₂/Al₂O₃ ratio = 50 mol mol⁻¹. It was observed that the H-ZSM-5-(50) non-impregnated catalyst has mainly strong Brønsted acid sites, and a few amount of strong Lewis acid sites.

The P impregnation produced some weak Lewis acid sites, while the few existing strong Lewis acid sites remained unchanged. On the other hand, Brønsted acid sites (strong and weak) had a slight increase. This caused

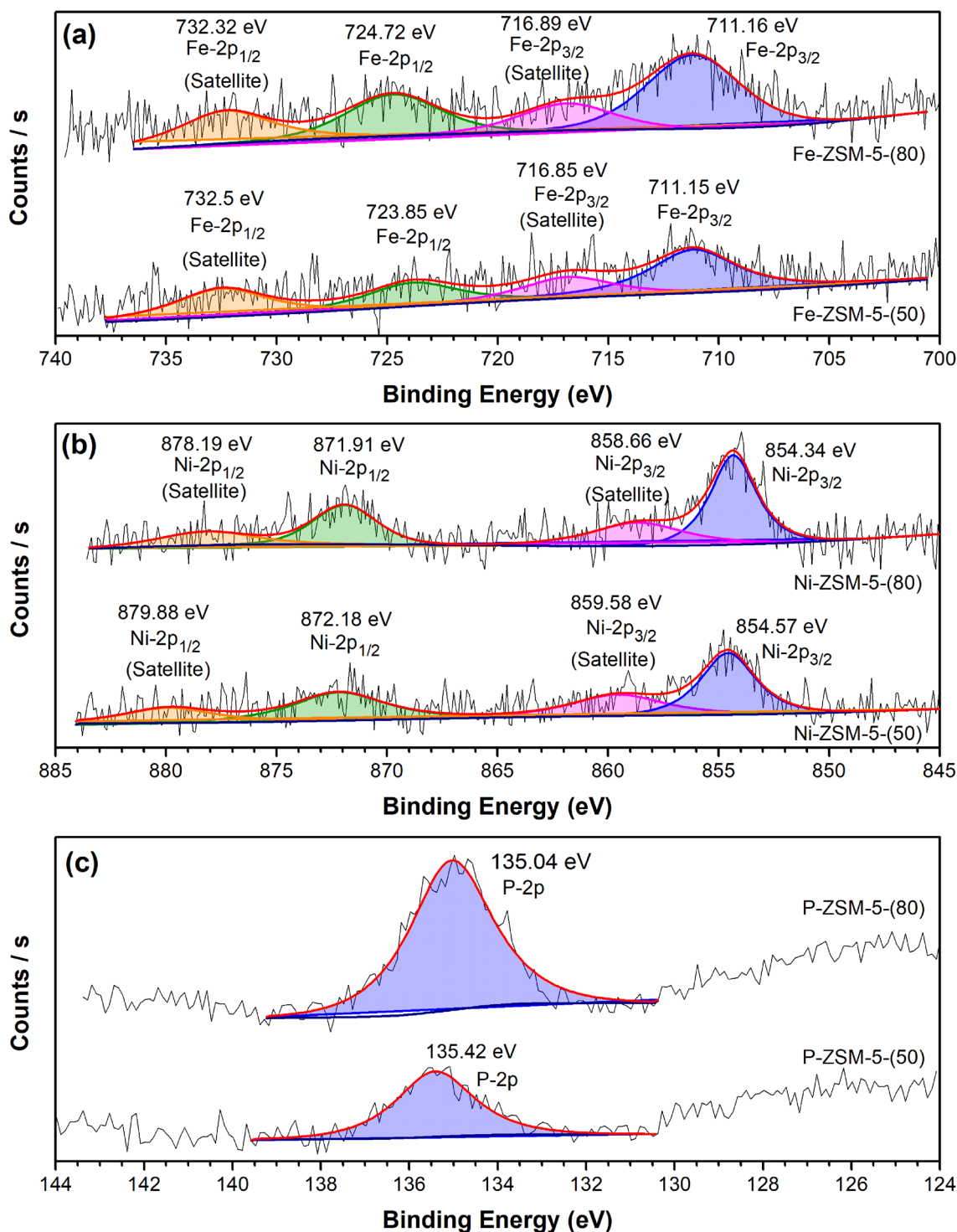


Fig. 4 XPS spectra of H-ZSM-5 catalysts impregnated with 1 wt% of Fe, Ni, and P. Deconvoluted configurations of: **a** Fe-2p, **b** Ni-2p and **c** P-2p

the total concentration of acid sites to be higher compared to the non-impregnated zeolite. Therefore, the concentration of acid sites, after P impregnation, corresponds predominantly to strong Brønsted sites, with an amount of

Lewis acid sites (strong + weak) slightly larger than in the non-impregnated zeolite.

The Fe impregnation did not significantly change the concentration of the Brønsted acid sites (strong and weak) originally existing in the ZSM-5 zeolite, but the Lewis acid

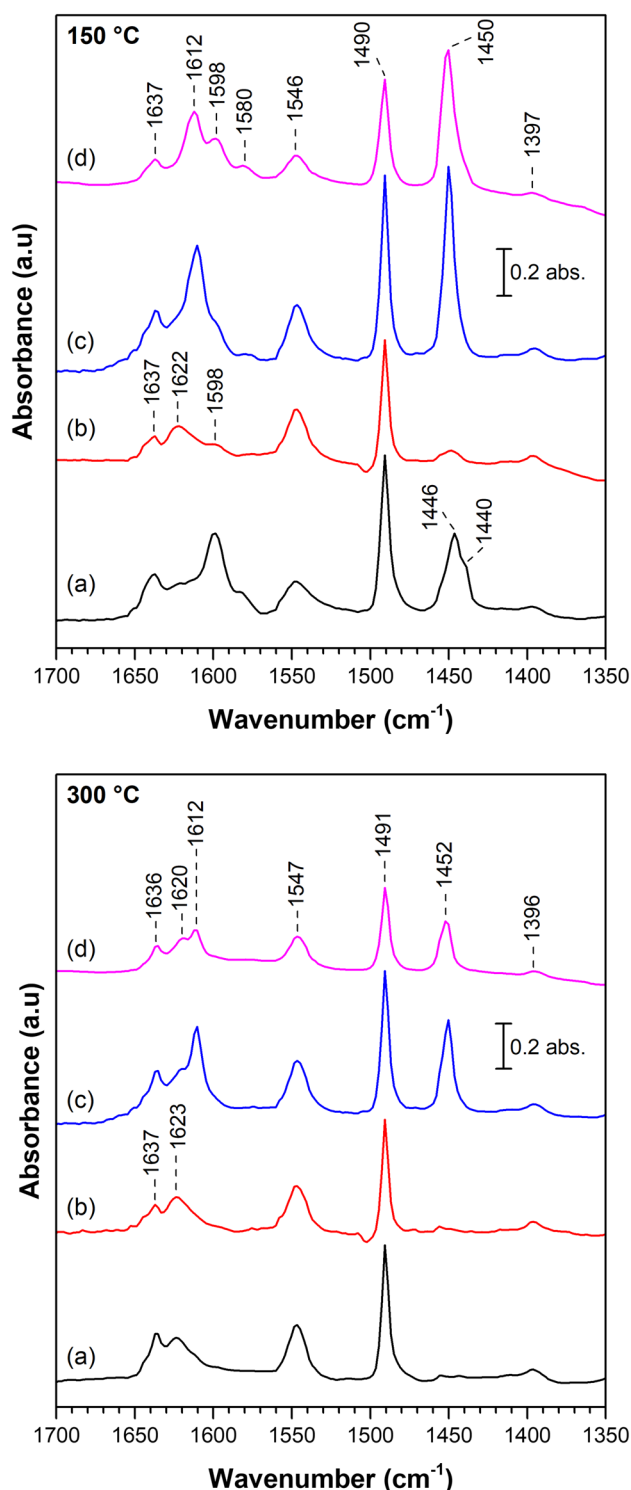


Fig. 5 FTIR difference spectra of adsorbed pyridine after evacuation at 150 °C and at 300 °C for the samples: **a** H-ZSM-5-(50), **b** P-ZSM-5-(50), **c** Fe-ZSM-5-(50), and **d** Ni-ZSM-5-(50)

sites (strong and weak) increased considerably along with the total concentration of acid sites. This is attributed to that the Fe_2O_3 particles impregnated on the surface carry

Lewis acidity, which is consistent with previous reports [27]. Therefore, the total acidity of the obtained catalyst corresponds mostly to Lewis acid sites with similar concentration of strong and weak sites, while Brønsted acid sites are mainly of the strong type but are available in lower concentration.

After Ni impregnation, the concentration of strong Brønsted acid sites decreased while that of the Lewis acid sites (strong and weak) increased, compared to the non-impregnated zeolite. On the other hand, the weak Brønsted acid sites did not undergo a significant change in their concentration, obtaining a very slight increase. It has been reported [51] that this change in the acidic property of ZSM-5 zeolite after Ni loading is because some Ni species perform ion exchange with the Brønsted acid sites, while the Lewis acid sites are generated on the small Ni particles dispersed in the zeolite channels. Because of the above, the total concentration of acid sites after Ni impregnation increased more than with the P loading, although not as much as with the Fe addition. The acidity of the obtained catalyst corresponds mostly to Lewis acid sites (being the weak Lewis sites the more abundant), while Brønsted acid sites are mainly of the strong type but are available in lower concentration than in the other three catalysts.

3.2 Catalytic Activity Testing

The catalytic activity of the catalysts and, specially, their selectivity to hydrocarbons was studied. In addition, the product distribution by carbon number was determined by carrying out the mass balance (liquid + gas) of the products. In all the reactions, because of the operating temperature (350 °C), the ethanol conversion was close to 100%, as reported in the literature [7, 9, 12], producing olefins, paraffins, naphthenes, aromatics and, in some cases, diethyl-ether. It was found that the non-impregnated H-ZSM-5-(50) catalyst had the highest mass yield of liquid hydrocarbons accumulated in 5 h of reaction (Fig. 6), obtaining the following global product yields: about ~28.9 wt% of the reacted ethanol was converted to liquid hydrocarbons, ~32 wt% to gas products and ~39.1 wt% to water. The activity of this catalyst was more favorable for the formation of condensable hydrocarbons (large molecules), mainly paraffins and aromatics. However, the product selectivity was strongly changing over time (Fig. 7a to f), which is attributed to a fast deactivation by coke deposition and low hydrothermal stability [52]. Initially, the selectivity values of C_{3+} olefins and ethylene were very low and increased progressively over time, while the formation of paraffins and aromatics was decreasing. It shows that the non-impregnated catalysts are unstable and several hours of reaction are needed to stabilize their catalytic activity.

Table 2 Concentration of Brønsted and Lewis acid sites expressed as micromoles of pyridine species per gram of sample ($\mu\text{mol g}^{-1}$), and its acid strength distribution (in percentage). Catalysts with $\text{SiO}_2/\text{Al}_2\text{O}_3$ ratio = 50 mol mol⁻¹

Catalyst	Weak acid sites ($\mu\text{mol g}^{-1}$)			Strong acid sites ($\mu\text{mol g}^{-1}$)			Brønsted acid sites strength (%)		Lewis acid sites strength (%)	
	$n_{\text{Brønsted}}^a$	n_{Lewis}^a	$n_{\text{B}} + n_{\text{L}}^c$	$n_{\text{Brønsted}}^b$	n_{Lewis}^b	$n_{\text{B}} + n_{\text{L}}^c$	B_{strong}^d	B_{weak}^d	L_{strong}^d	L_{weak}^d
H-ZSM-5-(50)	4.93	0.00	4.93	232.52	26.27	258.79	97.93	2.07	100.00	0.00
P-ZSM-5-(50)	32.51	25.71	58.22	261.26	24.98	286.24	88.93	11.07	49.28	50.72
Fe-ZSM-5-(50)	53.49	230.33	283.81	265.32	226.92	492.24	83.22	16.78	49.63	50.37
Ni-ZSM-5-(50)	8.67	300.62	309.30	132.82	123.08	255.91	93.87	6.13	29.05	70.95

^aConcentration of weak acid sites. Calculated by subtracting the strong acid sites from the total concentration of acid sites obtained after pyridine desorption at 150 °C. ($n_{\text{B}_{\text{weak}}} = n_{\text{B}_{150\text{ °C}}} - n_{\text{B}_{300\text{ °C}}}$) and ($n_{\text{L}_{\text{weak}}} = n_{\text{L}_{150\text{ °C}}} - n_{\text{L}_{300\text{ °C}}}$)

^bConcentration of strong acid sites after pyridine desorption at 300 °C

^cTotal concentration of acid sites (Brønsted + Lewis)

^dThe strength of Brønsted and Lewis acid sites is expressed as percentage distribution of strong and weak sites

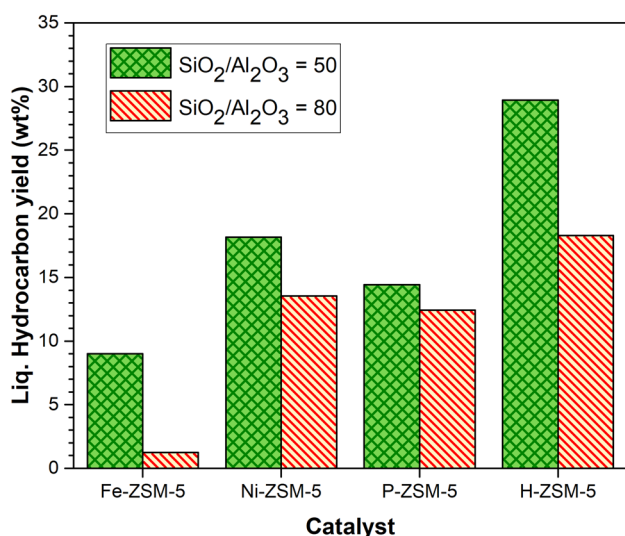


Fig. 6 Liquid hydrocarbon yield, accumulated in 5 h of reaction. P = 35 bar, T = 350 °C, WHSV = 10 ($\text{g}_{\text{EtOH}} \text{g}_{\text{cat}}^{-1} \text{h}^{-1}$)

The impregnated catalysts had a more stable product selectivity over time, compared to the non-impregnated materials. The P-ZSM-5-(50) catalyst obtained the highest selectivity to total olefins (Fig. 7a), mainly C_{3+} olefins (Fig. 7b) with a maximum of 70.8 wt% and 48.8 wt%, respectively, and the lower selectivity to ethylene (22.1 wt%) (Fig. 7c), at 3 h of reaction (TOS = 180 min), compared with the rest of the impregnated catalysts. The product yields show that a maximum of ~29.6 wt% of the fed ethanol was transformed to C_{3+} olefins and ~13.5 wt% to ethylene at 3 h of reaction. Likewise, the Fe-ZSM-5-(50) catalyst also exhibited a good selectivity for these products, although it produced more ethylene than the P-ZSM-5-(50) catalyst. In contrast, the P-ZSM-5-(80) catalyst showed the lowest selectivity to

olefins among the impregnated materials (Table 3). This was because the low acidity of H-ZSM-5-(80) zeolite ($\text{SiO}_2/\text{Al}_2\text{O}_3$ molar ratio = 80) was further reduced by impregnation of an alkaline compound such as phosphorus, and therefore its ability to form olefins and other hydrocarbons decreased. In general, it was observed that the C_{3+} olefin production decayed slightly over time with all the impregnated catalysts, while the ethylene formation increased.

Regarding the side products formation by the impregnated catalysts with $\text{SiO}_2/\text{Al}_2\text{O}_3$ molar ratio = 50, it was found that the P-ZSM-5-(50) catalyst produced the lowest amount of paraffins, while the Ni-ZSM-5-(50) catalyst produced more aromatics (Fig. 7c, e and f). In addition, the naphthene selectivity was less than 6.5 wt% for all the materials. Meanwhile, the H-ZSM-5-(50) non-impregnated catalyst produced a greater quantity of side products, which indicates that the impregnation improved the selectivity of this zeolite. Similar results were found by Ferreira et al. [53], who stated that undesired reactions and coke deposition are reduced because the impregnation favors the passivation of the strong Brønsted acid sites and therefore the hydrogen-transfer becomes limited. In particular, Song et al. [54] suggest that although strong acid sites are essential for the main reactions, a high concentration of strong acid sites favors side reactions such as hydrogen transfer or cyclization and eventually increase the formation of coke precursors; likewise, weak acid sites favor the alkenes methylation/cracking cycle. In contrast to the above, because of its low acidity, the side product selectivity for the catalysts with $\text{SiO}_2/\text{Al}_2\text{O}_3$ molar ratio = 80 was different. In this case, the phosphorus impregnation caused a higher formation of paraffins and aromatics with respect to the H-ZSM-5-(80) non-impregnated catalyst, while only the impregnation of iron did reduce the production of these side products. These results suggest that the catalyst acidity is the variable with the greatest influence on the product

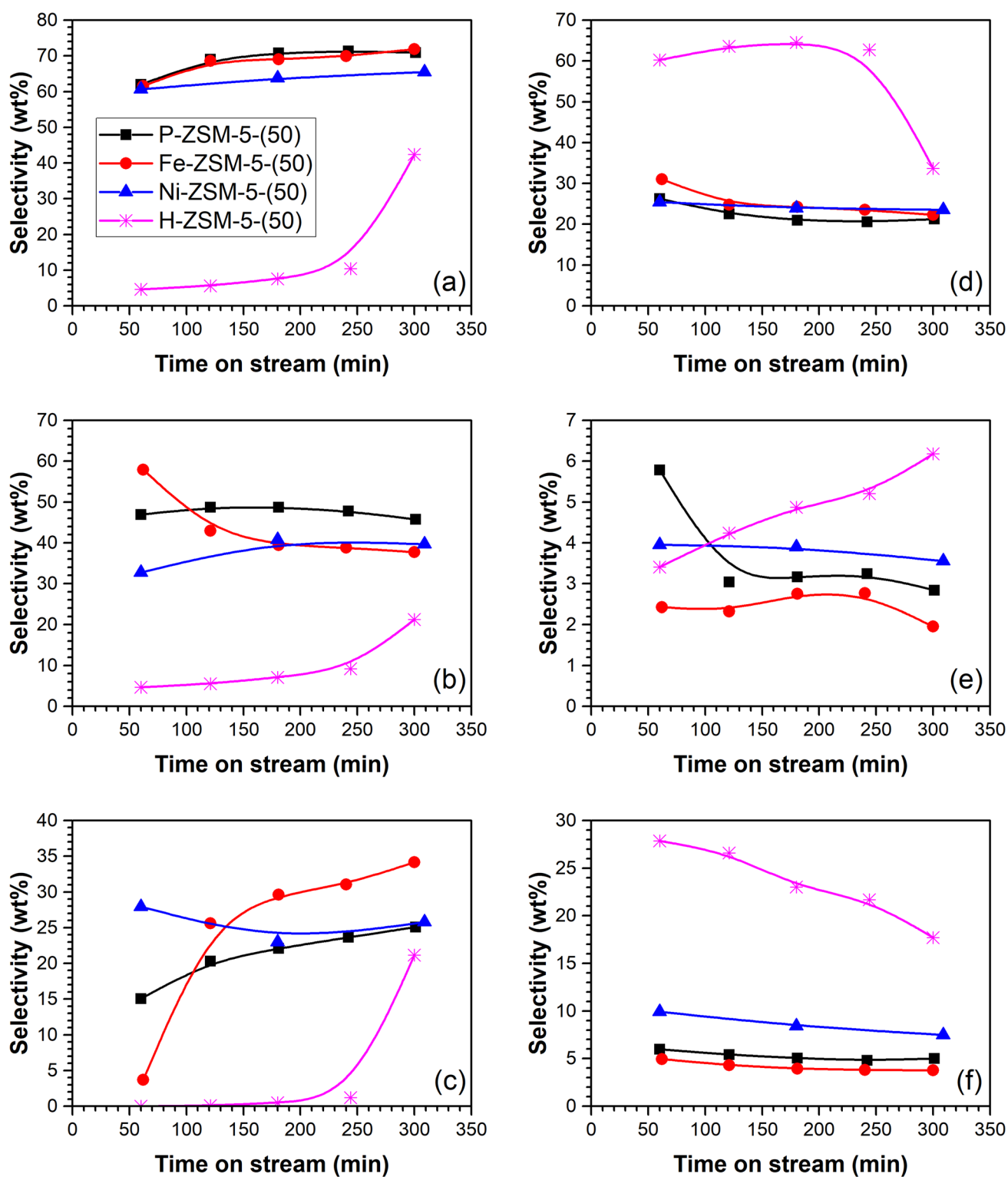


Fig. 7 Hydrocarbon selectivity over time on stream. Balance on a dry basis. **a** Total olefins (C_{3+} olefins + ethylene). **b** C_{3+} Olefins. **c** Ethylene. **d** Paraffins. **e** Naphthenes. **f** Aromatics. $P=35$ bar, $T=350$ °C, $WHSV=10$ ($l_{EtOH} g_{cat}^{-1} h^{-1}$). $SiO_2/Al_2O_3=50$ mol mol $^{-1}$

Table 3 Product selectivity per catalyst at 5 h of reaction. P=35 bar, T=350 °C, and WHSV = 10 ($\text{g}_{\text{EtOH}} \text{g}_{\text{cat}}^{-1} \text{h}^{-1}$)

	Catalyst							
	H-ZSM-5-(50)	P-ZSM-5-(50)	Fe-ZSM-5-(50)	Ni-ZSM-5-(50)	H-ZSM-5-(80)	P-ZSM-5-(80)	Fe-ZSM-5-(80)	Ni-ZSM-5-(80)
Product selectivity (wt%)								
Ethylene	21.14	25.09	34.18	25.79	30.98	25.80	53.85	34.48
n-Olefins C ₃₊	5.99	9.28	7.93	9.23	9.90	3.23	8.30	6.89
Iso-Olefins C ₃₊	15.31	36.50	29.82	30.44	24.69	2.75	15.45	15.89
n-Paraffins	11.59	6.27	8.19	8.26	9.16	10.16	8.00	3.71
Iso-Paraffins	22.08	14.99	14.14	15.26	14.10	26.64	10.96	12.47
Naphthenes	6.18	2.84	1.96	3.55	3.83	2.55	0.26	2.70
Alkylated aromatics	17.69	5.02	3.78	7.49	7.35	11.20	0.62	6.94
Diethyl-ether (DEE)	0.00	0.00	0.00	0.00	0.00	17.41	2.56	16.79
Others	0.00	0.00	0.00	0.00	0.00	0.26	0.00	0.14
Selectivity by carbon number (wt%)								
C2	21.71	25.60	34.56	26.52	31.51	26.22	54.38	34.93
C3	3.75	3.28	2.97	2.32	3.18	2.21	1.81	1.42
C4	11.84	20.79	20.39	20.88	15.21	34.42	20.41	27.91
C5	16.20	18.31	15.05	14.00	15.79	10.97	9.04	6.17
C6	13.02	8.84	9.44	10.42	9.95	5.63	7.91	6.04
C7	10.32	7.16	4.48	5.12	7.52	3.64	3.20	2.73
C8	9.39	5.97	3.57	7.68	6.33	4.12	0.39	4.24
C9	7.21	5.83	5.56	6.68	5.63	5.43	2.05	7.51
C10	5.12	3.43	3.03	4.98	4.03	4.88	0.63	6.68
C11	1.07	0.65	0.68	1.07	0.76	1.64	0.13	1.77
C12	0.29	0.09	0.17	0.24	0.06	0.59	0.03	0.41
C13	0.07	0.03	0.08	0.07	0.03	0.14	0.01	0.13
C14	0.00	0.01	0.02	0.01	0.00	0.09	0.00	0.04
C15	0.00	0.00	0.00	0.00	0.00	0.02	0.00	0.00

selectivity, while the impregnation of P, Fe and Ni specifically modified the type and concentration of the available acid sites, resulting in some catalysts being more selective to C₃₊ olefins and forming less side products than others.

With all the catalysts, most of the products were branched compounds (Table 3). Particularly, the produced alkylated aromatics include molecules such as toluene, (o, m, p)-xylene and larger. The diethyl-ether (DEE) molecule was produced only by the impregnated catalysts with SiO₂/Al₂O₃ molar ratio = 80 (Table 3), while none of the catalysts with SiO₂/Al₂O₃ ratio = 50 formed this compound. This was because the lower acidity of the P-HZSM-5-(80), Fe-HZSM-5-(80) and Ni-HZSM-5-(80) catalysts, and their reduced availability of Brønsted acid sites, limited the dehydration reaction of ethanol to ethylene, producing DEE as intermediate.

In Fig. 8, the (products/side products) selectivity ratios are plotted, where the higher the ratio value, the greater the

formation of the desired products and the lower the formation of side products. A comparison of the production of C₃₊ olefins and total olefins, relative to the preponderant side products (paraffins and aromatics), confirmed that the P-ZSM-5-(50) and Fe-ZSM-5-(50) catalysts were the most selective (Fig. 8a and c). However, the Fe-ZSM-5-(50) catalyst produced more ethylene than P-ZSM-5-(50) (Fig. 8b). On the other hand, the catalyst Fe-ZSM-5-(80) allowed to obtain a low formation of paraffins and aromatics relative to the production of total olefins (Fig. 8c), but this catalyst produced mainly ethylene, as well as a few amount of DEE (Table 3), so its selectivity to C₃₊ olefins was not the best (Fig. 8a). This confirms that the P-ZSM-5-(50) phosphorus catalyst was much more stable and selective to C₃₊ olefins than the Fe-ZSM-5-(50) iron catalyst, and therefore it was the material with the best activity. On the other hand, the P-ZSM-5-(80) phosphorous catalyst was the least

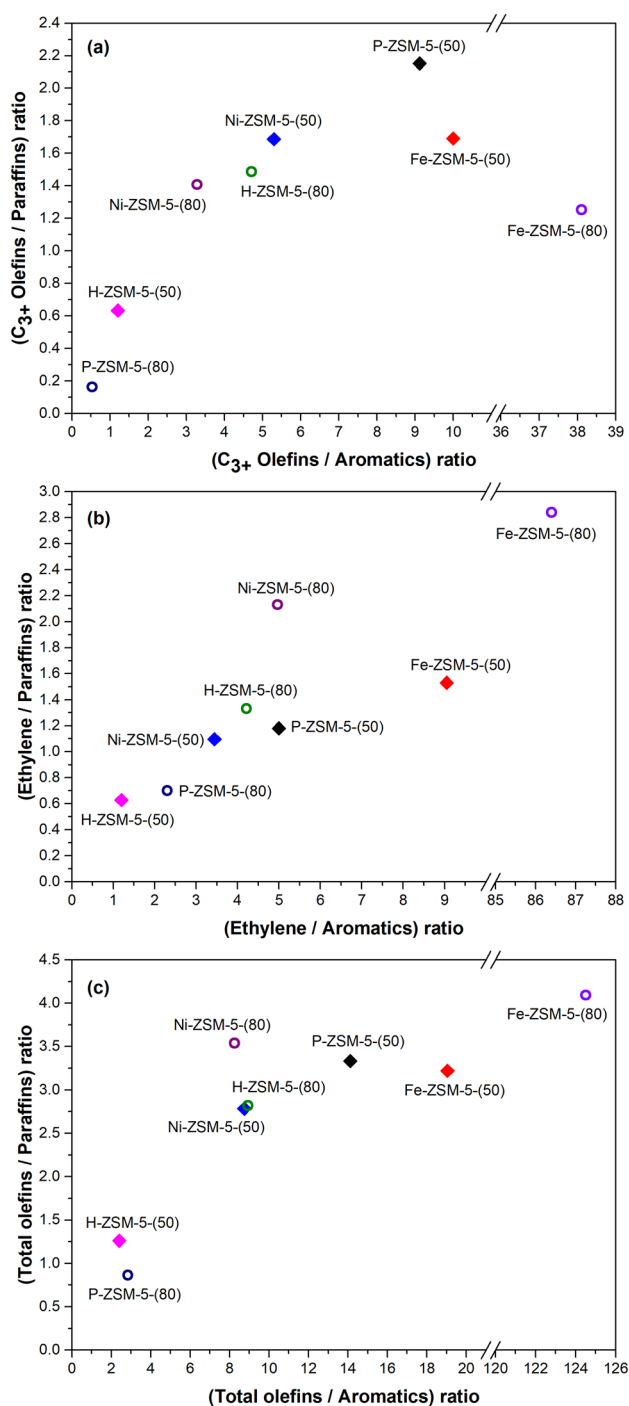


Fig. 8 Plots of (products/side products) selectivity ratios at 5 h of reaction. Comparison of catalysts. **a** C₃₊ olefin production relative to the formation of aromatics and paraffins. **b** Ethylene production relative to the formation of aromatics and paraffins. **c** Total olefin production (ethylene + C₃₊ olefins) relative to the formation of aromatics and paraffins. P = 35 bar, T = 350 °C, WHSV = 10 (g_{EtOH} g_{cat}⁻¹ h⁻¹)

selective to olefins, and even more, it was the catalyst that produced the highest amount of DEE, just followed by the Ni-ZSM-5-(80) nickel catalyst as shown in Table 3.

4 Conclusions

The P, Fe, and Ni impregnation did not modify the morphology or the crystallographic properties of the ZSM-5 zeolite. The particles were adhered and well dispersed on the surface, producing a slight decrease in the apparent BET area and the micropores volume. Additionally, the XPS analysis indicated that the Fe particles correspond to Fe₂O₃, those of Ni correspond to NiO and those of phosphorus to P₂O₅. No evidence of a possible incorporation of P to the structure of ZSM-5 zeolite was found by XPS. On the other hand, the impregnation of P, Fe, and Ni caused significant changes in the strength and concentration of the Brønsted and Lewis acid sites, and therefore strongly influenced the selectivity to C₃₊ olefins.

The evaluated catalysts were able to transform the ethanol to hydrocarbons + water, where the hydrocarbons obtained were: n-olefins (n-alkenes), iso-olefins (branched alkenes), n-paraffins (n-alkanes), iso-paraffins (branched alkanes), naphthenes (cycloalkanes), and alkylated aromatics. The impregnation of P, Fe, and Ni on ZSM-5 zeolite with SiO₂/Al₂O₃ molar ratio = 50 proved to be effective and substantially improved the activity and stability of the catalysts, achieving selectivities to olefins higher than that obtained with the non-impregnated catalyst. In contrast, for the ZSM-5 zeolite with SiO₂/Al₂O₃ molar ratio = 80, the selectivity was only improved with the addition of iron, but was worsened by impregnating phosphorus and nickel. This was because of the change in the concentration and strength of the acid sites in the ZSM-5 zeolites after impregnation, which confirms that the selectivity to C₃₊ olefins was strongly influenced by the acidity of the catalysts. The materials with SiO₂/Al₂O₃ molar ratio = 50 were better than those of 80, obtaining the highest selectivity to C₃₊ olefins and the lowest selectivity to side products (paraffins and aromatics) in the following order: P-ZSM-5-(50) > Fe-ZSM-5-(50) > Ni-ZSM-5-(50) > Fe-ZSM-5-(80) > H-ZSM-5-(80) > Ni-ZSM-5-(80) > P-ZSM-5-(80).

Particularly, for the ZSM-5 zeolite with SiO₂/Al₂O₃ molar ratio = 50, the P addition allows to obtain a catalyst with acidity predominantly of strong Brønsted type, and with higher concentration of total acid sites in comparison with the non-impregnated zeolite, producing some weak Lewis sites. On the other hand, the impregnated Fe particles produced Lewis acid sites, which allows to obtain a catalyst mainly with a balanced Lewis acidity (strong + weak). And finally, Ni particles partially decreased the strong Brønsted sites, as well as behaved as Lewis acid sites, allowing to obtain a catalyst mainly with Lewis acidity (weak Lewis sites being the more abundant). This suggests that all the reactions for hydrocarbon formation were carried out at both Brønsted and Lewis acid sites, but it was the

Brønsted sites that mostly promoted the ethanol dehydration and ethylene oligomerization, as well as the side reactions. Particularly, the aromatization and hydrogen transfer reactions were reduced when the strength of both Brønsted and Lewis acid sites decreased. It demonstrates the importance of the catalyst acidity for the production of hydrocarbons molecules different from ethylene, including condensable compounds.

Acknowledgements To National Council of Science and Technology (CONACYT) for the scholarship No. 221945 granted to Ricardo Gil for his doctoral studies. To the BIOTURBOSINA cluster, under support from CONACYT-SENER project No. 248090, for the resources granted to carry out this research. To National Laboratory of Nano and Biomaterials (LANNBIO), CINVESTAV-Mérida, under founding from projects FOMIX Yucatán 2008–108160 CONACYT LAB-2009–01-123913, 292692, 294643, for the facilities to perform the BET and XPS characterization analysis. To UNICAT-FQ-UNAM for the facilities to perform the FTIR acidity characterization. To Tanit Toledano Thompson (UER-CICY) for her technical assistance in SEM–EDX measurements.

Compliance with Ethical Standards

Conflict of interest The authors declare no conflict of interest.

References

- Lu J, Liu Y (2011) *J Nat Gas Chem* 20(2):162–166. [https://doi.org/10.1016/S1003-9953\(10\)60163-6](https://doi.org/10.1016/S1003-9953(10)60163-6)
- Inaba M, Murata K, Saito M, Takahara I (2007) *Green Chem* 9(6):638–646. <https://doi.org/10.1039/B614157A>
- Galadima A, Muraza O (2015) *J Ind Eng Chem* 31:1–14. <https://doi.org/10.1016/j.jiec.2015.07.015>
- Cherubini F (2010) *Ener Convers Manage* 51(7):1412–1421. <https://doi.org/10.1016/j.enconman.2010.01.015>
- Li X, Kant A, He Y, Thakkar HV, Atanga MA, Rezaei F, Ludlow DK, Rownaghi AA (2016) *Catal Today* 276:62–77. <https://doi.org/10.1016/j.cattod.2016.01.038>
- Renewable Fuels Association (2018) World fuel ethanol production. <https://ethanolrfa.org/statistics/annual-ethanol-production/>. Accessed 20 June 2019
- Sousa ZSB, Veloso CO, Henriques CA, Teixeira da Silva V (2016) *J Mol Catal a-Chem* 422:266–274. <https://doi.org/10.1016/j.molcata.2016.03.005>
- Kondo JN, Ito K, Yoda E, Wakabayashi F, Domen K (2005) *J Phys Chem B* 109(21):10969–10972. <https://doi.org/10.1021/jp050721q>
- Zhang X, Wang R, Yang X, Zhang F (2008) *Micropor Mesopor Mat* 116(1–3):210–215. <https://doi.org/10.1016/j.micromeso.2008.04.004>
- Nash CP, Ramanathan A, Ruddy DA, Behl M, Gjersing E, Griffin M, Zhu H, Subramaniam B, Schaidle JA, Hensley JE (2016) *Appl Catal A-Gen* 510:110–124. <https://doi.org/10.1016/j.apcata.2015.11.019>
- Madeira FF, Gnep NS, Magnoux P, Maury S, Cadran N (2009) *Appl Catal A-Gen* 367(1–2):39–46. <https://doi.org/10.1016/j.apcata.2009.07.033>
- Zhang D, Wang R, Yang X (2008) *Catal Lett* 124(3):384–391. <https://doi.org/10.1007/s10562-008-9481-x>
- Lu J, Liu Y, Li N (2011) *J Nat Gas Chem* 20(4):423–427. [https://doi.org/10.1016/S1003-9953\(10\)60193-4](https://doi.org/10.1016/S1003-9953(10)60193-4)
- Goto D, Harada Y, Furumoto Y, Takahashi A, Fujitani T, Oumi Y, Sadakane M, Sano T (2010) *Appl Catal A-Gen* 383(1–2):89–95. <https://doi.org/10.1016/j.apcata.2010.05.032>
- Takahashi A, Xia W, Nakamura I, Shimada H, Fujitani T (2012) *Appl Catal A-Gen* 423 (Supplement C):162–167. <https://doi.org/10.1016/j.apcata.2012.02.029>
- Song Z, Takahashi A, Mimura N, Fujitani T (2009) *Catal Lett* 131(3):364–369. <https://doi.org/10.1007/s10562-009-0071-3>
- Song Z, Takahashi A, Nakamura I, Fujitani T (2010) *Appl Catal A-Gen* 384(1–2):201–205. <https://doi.org/10.1016/j.apcata.2010.06.035>
- Inaba M, Murata K, Takahara I (2009) *React Kinet Catal Lett* 97(1):19–26. <https://doi.org/10.1007/s11144-009-0002-8>
- Inaba M, Murata K, Takahara I, Inoue K (2011) *J Chem Technol Biotechnol* 86(1):95–104. <https://doi.org/10.1002/jctb.2519>
- Inaba M, Murata K, Takahara I, Inoue K (2012) *Adv Mater Sci Eng* 2012:7. <https://doi.org/10.1155/2012/293485>
- Gayubo AG, Alonso A, Valle B, Aguayo AT, Bilbao J (2010) *Appl Catal B-Environ* 97(1–2):299–306. <https://doi.org/10.1016/j.apcatb.2010.04.021>
- Furumoto Y, Harada Y, Tsunoji N, Takahashi A, Fujitani T, Ide Y, Sadakane M, Sano T (2011) *Appl Catal A-Gen* 399(1):262–267. <https://doi.org/10.1016/j.apcata.2011.04.009>
- Ouyang J, Kong F, Su G, Hu Y, Song Q (2009) *Catal Lett* 132(1):64–74. <https://doi.org/10.1007/s10562-009-0047-3>
- Tretyakov VF, Makarfi YI, Tretyakov KV, Frantsuzova NA, Talyshinskii RM (2010) *Catal ind* 2(4):402–420. <https://doi.org/10.1134/s2070050410040161>
- Makarfi YI, Yakimova MS, Lermontov AS, Erofeev VI, Koval LM, Tretyakov VF (2009) *Chem Eng J* 154(1–3):396–400. <https://doi.org/10.1016/j.cej.2009.06.001>
- Gayubo AG, Alonso A, Valle B, Aguayo AT, Olazar M, Bilbao J (2010) *Fuel* 89(11):3365–3372. <https://doi.org/10.1016/j.fuel.2010.03.002>
- Phung TK, Radikapratama R, Garbarino G, Lagazzo A, Riani P, Busca G (2015) *Fuel Process Technol* 137:290–297. <https://doi.org/10.1016/j.fuproc.2015.03.012>
- Van der Borght K, Galvita VV, Marin GB (2015) *Appl Catal A-Gen* 492:117–126. <https://doi.org/10.1016/j.apcata.2014.12.020>
- Leofanti G, Padovan M, Tozzola G, Venturelli B (1998) *Catal Today* 41(1):207–219. [https://doi.org/10.1016/S0920-5861\(98\)00050-9](https://doi.org/10.1016/S0920-5861(98)00050-9)
- McCue AJ, Mutch GA, McNab AI, Campbell S, Anderson JA (2016) *Catal Today* 259:19–26. <https://doi.org/10.1016/j.cattod.2015.03.039>
- Pieta IS, Ishaq M, Wells RPK, Anderson JA (2010) *Appl Catal A-Gen* 390(1):127–134. <https://doi.org/10.1016/j.apcata.2010.10.001>
- Emeis CA (1993) *J Catal* 141(2):347–354. <https://doi.org/10.1006/jcat.1993.1145>
- Barzetti T, Selli E, Moscotti D, Forni L (1996) *J Chem Soc. Faraday Trans* 92(8):1401–1407. <https://doi.org/10.1039/FT9969201401>
- Li X, Han D, Wang H, Liu G, Wang B, Li Z, Wu J (2015) *Fuel* 144:9–14. <https://doi.org/10.1016/j.fuel.2014.12.005>
- Haw JF (2002) *Phys Chem Chem Phys* 4(22):5431–5441. <https://doi.org/10.1039/B206483A>
- Singh R, Dutta PK (2003) MFI: a case study of zeolite synthesis. In: Auerbach SM, Carrado KA, Dutta PK (eds) *Handbook of zeolite science and technology*. Marcel Dekker, Inc., New York. <https://doi.org/10.1201/9780203911167>

37. Rasouli M, Atashi H, Mohebbi-Kalhari D, Yaghobi N (2017) *J Taiwan Inst Chem E* 78:438–446. <https://doi.org/10.1016/j.jtice.2017.05.018>
38. Armaroli T, Simon LJ, Digne M, Montanari T, Bevilacqua M, Valtchev V, Patarin J, Busca G (2006) *Appl Catal A-Gen* 306:78–84. <https://doi.org/10.1016/j.apcata.2006.03.030>
39. Biesinger MC, Payne BP, Grosvenor AP, Lau LWM, Gerson AR, Smart RSC (2011) *Appl Surf Sci* 257(7):2717–2730. <https://doi.org/10.1016/j.apsusc.2010.10.051>
40. Yamashita T, Hayes P (2008) *Appl Surf Sci* 254(8):2441–2449. <https://doi.org/10.1016/j.apsusc.2007.09.063>
41. Grosvenor AP, Kobe BA, Biesinger MC, McIntyre NS (2004) *Surf Interface Anal* 36(12):1564–1574. <https://doi.org/10.1002/sia.1984>
42. Kraushofer F, Jakub Z, Bichler M, Hulva J, Drmota P, Weinold M, Schmid M, Setvin M, Diebold U, Blaha P, Parkinson GS (2018) *J Phys Chem C* 122(3):1657–1669. <https://doi.org/10.1021/acs.jpcc.7b10515>
43. Mansour AN, Brizzolara RA (1996) *Surf Sci Spectra* 4(4):351–356. <https://doi.org/10.1116/1.1247832>
44. Mansour AN (1994) *Surf Sci Spectra* 3(3):231–238. <https://doi.org/10.1116/1.1247751>
45. Wang Y, Sherwood PMA (2002) *Surf Sci Spectra* 9(1):159–165. <https://doi.org/10.1116/11.20030115>
46. Sherwood PMA (2002) *Surf Sci Spectra* 9(1):62–66. <https://doi.org/10.1116/11.20030101>
47. Blasco T, Corma A, Martínez-Triguero J (2006) *J Catal* 237(2):267–277. <https://doi.org/10.1016/j.jcat.2005.11.011>
48. Zhuang J, Ma D, Yang G, Yan Z, Liu X, Liu X, Han X, Bao X, Xie P, Liu Z (2004) *J Catal* 228(1):234–242. <https://doi.org/10.1016/j.jcat.2004.08.034>
49. Marques JP, Gener I, Ayrault P, Bordado JC, Lopes JM, Ramôa Ribeiro F, Guisnet M (2003) *Micropor Mesopor Mat* 60(1):251–262. [https://doi.org/10.1016/S1387-1811\(03\)00382-2](https://doi.org/10.1016/S1387-1811(03)00382-2)
50. Busca G (2017) *Micropor Mesopor Mat* 254:3–16. <https://doi.org/10.1016/j.micromeso.2017.04.007>
51. Suganuma S, Nakamura K, Okuda A, Katada N (2017) *Mol Catal* 435:110–117. <https://doi.org/10.1016/j.mcat.2017.03.029>
52. Aguayo AT, Gayubo AG, Atutxa A, Olazar M, Bilbao J (2002) *Ind Eng Chem Res* 41(17):4216–4224. <https://doi.org/10.1021/ie020068i>
53. Ferreira Madeira F, Gnep NS, Magnoux P, Vezin H, Maury S, Cadran N (2010) *Chem Eng J* 161(3):403–408. <https://doi.org/10.1016/j.cej.2010.01.026>
54. Song Y, Zhang L, Li G, Shang Y, Zhao X, Ma T, Zhang L, Zhai Y, Gong Y, Xu J, Deng F (2017) *Fuel Process Technol* 168:105–115. <https://doi.org/10.1016/j.fuproc.2017.08.020>

Publisher's Note Springer Nature remains neutral with regard to jurisdictional claims in published maps and institutional affiliations.